# PASSIVE CONTROL OF THE SEPARATION INDUCED BY CONVEX GEOMETRY AT HIGH REYNOLDS NUMBER

**Artur Dróżdż**
Department of Thermal Machinery
Czestochowa University of Technology
Armii Krajowej 21, 42-200, Czestochowa
artur.drozdz@pcz.pl

**Mathias Romańczyk**
Department of Thermal Machinery
Czestochowa University of Technology
Armii Krajowej 21, 42-200, Czestochowa
mathias.romanczyk@pcz.pl

**Witold Elsner**
Department of Thermal Machinery
Czestochowa University of Technology
Armii Krajowej 21, 42-200, Czestochowa
witold.elsner@pcz.pl

## ABSTRACT

The paper presents a high Reynolds number experimental study of turbulent boundary layer separation control on a convex plate using the wavy-wall method, which was initially proposed for a flat plate by Dróżdż et al. 2021 (Exp Therm Fluid Sci 2021;121:110291). The application of this method increases the friction coefficient by up to 42.3%, resulting in a substantial delay in turbulent separation from the convex wall, while maintaining total momentum, quantified by changes in momentum-loss thickness. Other parameters indicating the high efficiency of the method are the invariant value of the friction Reynolds number along the flow and the thinner boundary layer. The above indicators demonstrate promising aerodynamic improvements in airfoils, similar to those achieved when active suction is applied to the suction side. The new insight into the physical mechanism of the wavy wall suggests that small-scale turbulent activity is the primary determinant of the effectiveness of the wavy wall in enhancing small-scale streamwise convection and the sweeping motion, resulting in superior momentum transport.

## INTRODUCTION

Most passive flow control strategies for aerofoils are based on reducing skin friction by attenuating large-scale streaks (Ricco *et al.*, 2021). To mitigate skin friction reduction, which acts as a laminar-turbulent transition postponer, active methods are employed to counteract its detrimental effect on lift due to earlier separation. However, the use of active methods is limited in wind turbine blades due to a combination of practical, aerodynamic, and economic constraints. A commonly applied passive method in wind energy is the use of vortex generators. However, in large-scale wind turbine blades, vortex generators provide only minimal benefits (only about a 1% power increase on 5MW wind turbine blades). They may even lower efficiency at higher power levels (Bravo-Mosquera *et al.*, 2022). Alternative passive flow control methods such as dimples (Tay *et al.*, 2015; Gattere *et al.*, 2022; Aoki *et al.*, 2012; Bearman & Harvey, 1976; Tay, 2011), grooves (S. & H., 2016), slotted airfoils (Belamadi *et al.*, 2016; Coder & Somers, 2020; Tanürün *et al.*, 2026), or microcylinders (Wang *et al.*, 2018; Mostafa *et al.*, 2022; Wang *et al.*, 2023) have been shown to reduce drag by speeding up the transition; however, their effectiveness diminishes in turbulent flows with high Reynolds numbers as shown by McMasters & Henderson (1979).

A promising alternative is the use of a streamwise wavy wall (WW) with appropriately selected geometry that yields an increase in friction coefficient downstream of WW of more than 35% at the friction Reynolds number $Re_\tau \approx 4000$ (Dróżdż *et al.*, 2025). This is the highest reported gain for such a configuration to date, which highlights the practical potential of this method to delay separation. To be effective, the WW design must be carefully tailored to local flow conditions. The undulations should be placed where the Rotta-Clauser pressure gradient parameter $\beta = \delta^* \tau_w^{-1} dP_e$, where $\delta^*$ is displacement thickness, $\tau_w$ is wall shear stress and $dPe$ is streamwise pressure gradient, remains below 10, with a maintained viscous scaled amplitude of $A^+ = 170$, and a period adjusted so that flow troughs are held on the verge of separation (effective slope around 0.15). The wavy wall increases the momentum transport due to increased small-scale sweeping motions, in a mechanism similar to amplitude modulation in high-Reynolds wall-bounded flows (Mathis *et al.*, 2009; Dróżdż *et al.*, 2023). Simulations at about $Re_\tau \approx 2500$ by Kamiński *et al.* (2024) confirmed that the technique can enhance the wall-normal velocity gradient and wall shear stress downstream, although to a lesser extent. In turn, combined numerical LES and wind-tunnel studies by Elsner *et al.* (2022) at $Re_\tau \approx 1400$ did not show any improvements, suggesting the approach loses efficacy below a certain threshold Reynolds number.

The recent work of Dróżdż *et al.* (2025) aimed to test the single geometry of the WW selected in Dróżdż *et al.* (2021) on a range of Reynolds numbers ($Re_\tau \approx 2600$, 4000, and 4500) and under varying pressure gradient conditions corresponding to large-scale pitch-regulated wind turbine blades. For such turbines, the angle of attack varies from 3° to 8° Sayed *et al.* (2012) for different wind speeds, and even more due to the rotational position or torsional deflection of the blade. The results showed that when the Reynolds number varies, as when the wind speeds change from 5 to $40ms^{-1}$ on a pitch-regulated wind turbine, the lowest increase in $C_f$ was 30% for the lowest Reynolds number. Furthermore, when the pressure gradient was varied at a constant Reynolds number, mimicking unstable flow conditions resulting from changes in the rotational position of the blade or torsional deflection, the efficiency of the wavy wall was maintained, albeit at a lower level of $C_f$, about 27% on average. The tested pressure ranges and the Reynolds number variation showed that too low an amplitude limits the benefits. On the other hand, too high an amplitude leads to significant separation, weakening momentum transport to the wall. Nevertheless, as demonstrated, an overall effectiveness of approximately 23% was achieved, which can be considered high.

Recently, large-eddy simulations at $Re_\tau \approx 2500$ by Kamiński *et al.* (2025) was published as an extended work of Kamiński *et al.* (2024). They showed that the additional benefit can be achieved using the upstream tilted wavy wall (Kamiński *et al.*, 2025). They report an increase in wall shear stress with respect to a sinusoidal type of wavy wall. However, the increase is at the level of 40% of that observed in Dróżdż *et al.* (2021) due to the lower Reynolds number. In addition, Kamiński *et al.* (2025) presented their observations on the physical interpretation of introducing a wavy wall on the curved surface of the NACA4412 wing section. They found that a sinusoidal wavy wall used at $Re_\tau \approx 2500$ causes increased energy across all scales in the outer region. In contrast, near the wall, only large-scale activity is enhanced, despite the small-scale contribution observed by Dróżdż *et al.* (2021).

The experimental results in this paper document for the first time the application of the wavy wall on a convex surface that resembles a wind turbine blade surface at a high Reynolds number $Re_\tau \approx 3100$ corresponding to the wind speed $10ms^{-1}$ that occurs on a large-scale wind turbine blade that spins at a constant speed regulated by the blade pitch. The changes in velocity statistics and boundary-layer parameters produced by the method were compared with those obtained using the active techniques reported in the literature (Atzori *et al.*, 2020).

## EXPERIMENTAL SETUP

The experiment was carried out in a modular wind tunnel explicitly designed for studying wind turbine blades' surfaces under real atmospheric conditions located at Czestochowa University of Technology, where the canonical turbulent boundary layer (TBL) can develop up to a $7500mm$ long flat plate without tripping. The Reynolds number based on developing distance is $Re_x = 10^7$. The honeycomb-equipped settling chamber and the set of five turbulence grids, together with the contraction channel of contraction ratio of 4.5, ensure that the turbulence intensity 7.5 metres downstream in the inlet channel was not higher than 0.45%. To restrain the three-dimensional effects, i.e. secondary flows in the channel, the cross-section of the channel at the inlet was designed with the following $WxH$ dimensions: $416x800$ mm. Downstream the inlet channel, a curved surface section corresponds to the part of the NACA4412 profile suction side at the angle of attack (AoA) equal to 5° was installed (see Fig. 1). The part of the wing section corresponds from the higher point of the profile at $AoA = 5°$ to its trailing edge at the outlet of the wind tunnel.

In each case, the measurements were carried out downstream of the wavy surface and compared with the measurements without a wavy surface. The mean velocity and its fluctuation profiles were measured with a free-from-spatial-averaging hot-wire probe. The amplitude of WW $A(x)$ increases downstream of the flow according to the relationship: $A^+ = A(x)u_\tau \nu^{-1} = 170$, where $u_\tau$ is the friction velocity and $\nu$ is the kinematic viscosity.

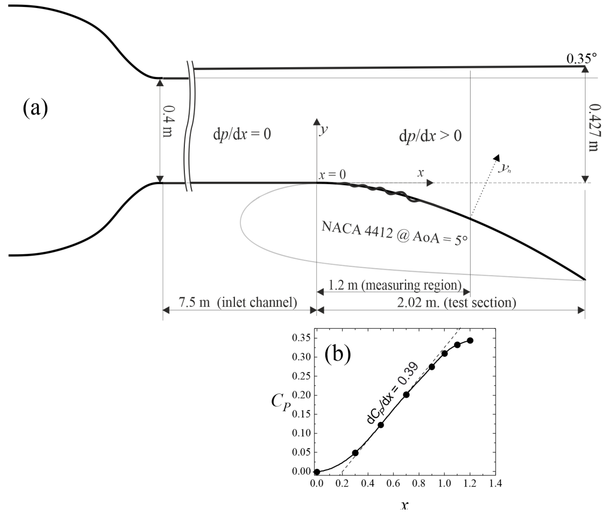


Figure 1. Schematic of the test section (a) and $C_p$ distributions (b)

Table 1. Inlet TBL parameters

| $z$ | $U_{e,in}$ | $\delta_{in}$ | $C_{f,in}$ |
|---|---|---|---|
| $(m)$ | $(ms^{-1})$ | $(mm)$ | $(-)$ |
| -0.2 | 14.58 | 98.4 | 0.00255 |
| -0.1 | 14.32 | 93.5 | 0.00259 |
| 0 | 14.33 | 90.5 | 0.00256 |
| 0.1 | 14.34 | 93.5 | 0.00255 |
| 0.2 | 14.48 | 91.9 | 0.00259 |

The distributions of the pressure coefficient $C_P = 1 - U_e^2 U_{e,in}^{-2}$ are shown in Figure 1b. It should be emphasised that the waviness, due to its low amplitude in relation to the height of the channel, does not affect the $C_P$ distribution in the freestream. The upper wall of the inlet channel was inclined at 0.35° to ensure maintaining the ZPG conditions. (see Fig. 1a).

The experiment was carried out for the value of the inlet velocity $U_{e,in} \approx 14.5ms^{-1}$, which corresponds to $Re_\tau \approx 3100$.

### Inlet Conditions

Table 1 contains inlet data for five velocity profiles distributed spanwise. For each case, a ◯ symbol colour has been assigned. It is important to note that the flow maintains well-behaved ZPG TBL flow conditions introduced by Sanmiguel Vila *et al.* (2017), as the skin friction coefficient $C_f$ and the shape factor $H$ for analysed $Re_{\theta,in} \approx 9700$ in the inner 50% of channel span do not exceed ±2% and ±1 of the Coles–Fernholz formula and the relation proposed by Monkewitz *et al.* (2007), respectively (see Figure (2a)).

Figure 2 shows the inlet profiles ($x = 0.0$ mm) of the mean velocity $U^+ = Uu_\tau^{-1}$ (2a) and the streamwise Reynolds stresses $\overline{uu}^+$ in the viscous units (2b), measured for five spanwise locations $z = -200$, 100, 0, 100 and 200 mm. Figure 2a) shows a canonical turbulent boundary layer at the inlet, while Figure 2b) shows that $\overline{uu}^+$ collapses under uncertainty of 5%.

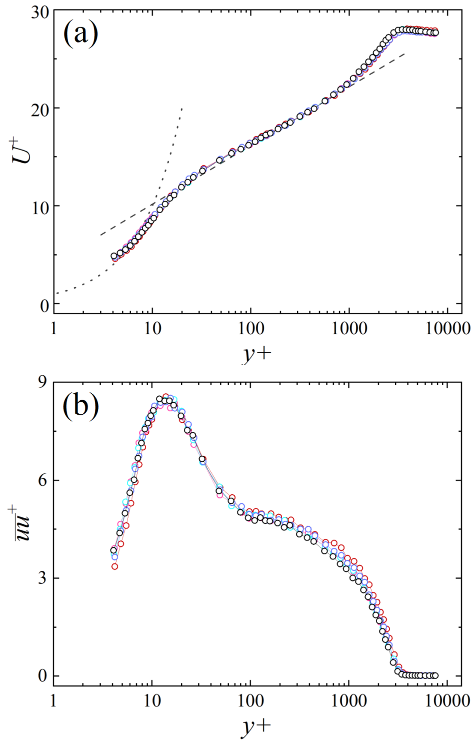


Figure 2. Mean velocity (a) and turbulence intensity (b) profiles presented in viscous scale at $x = 0$ and $z = 0$ black, $z = -100$ magenta, $z = 100$ cyan, $z = -200$ red, $z = 200$ blue. The dashed line represents the logarithmic law (with $\kappa = 0.38$ and $B = 4.1$) while the dotted line represents $y^+ = U^+$.

It confirms that the velocity profiles at the inlet were measured using a sufficiently short wire length to avoid measured small-scale energy attenuation.

## RESULTS

In Figure 3, the skin friction coefficient $C_f = 2u_\tau^2 U_e^{-2}$ for the wavy surface (open symbols) is compared to the unmodified wing surface $C_f$ (dark symbols), where a second-order polynomial extrapolated the distributions to predict the separation point. The streamwise distance from the inlet $x$ was reduced by the boundary layer thickness at the inlet $\delta_{in}$. The purple area indicates the flow region where the waviness is located. Figure 3 illustrates a marked enhancement in the skin-friction coefficient for the wavy wall configuration, as denoted by the open symbols. This increase is accompanied by a pronounced downstream displacement of the turbulent boundary layer separation point, indicating the efficacy of the wavy geometry in delaying flow detachment.

For a more statistically confident estimate of the effect of waviness on the skin friction coefficient, the differences between the $C_f$ distributions were integrated from the end of the wavy wall to the flow separation location occurring for the flow without surface modification. The integration area does not account for the tangential separation shift $\Delta x_{t,s}$. The percentage value of $\Delta C_f$ was scaled by $C_{f,in}$ to assess the real effectiveness of the method.

The data in Table 2 show that the selected corrugation geometry produces an increase of 42.3% in $C_f$ in the integration area downstream of the wavy wall.

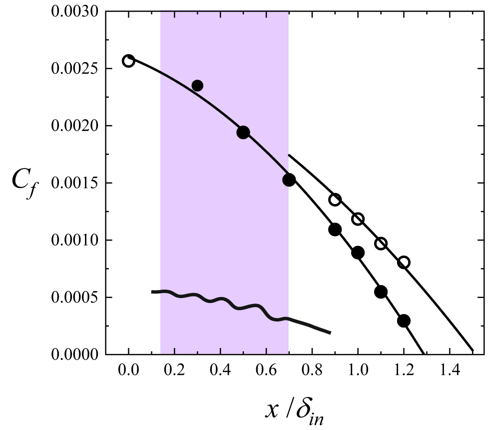


Figure 3. Comparison of skin-friction coefficient distributions. The open symbol corresponds to the wavy wall, while the dark symbol corresponds to the unmodified wing surface.

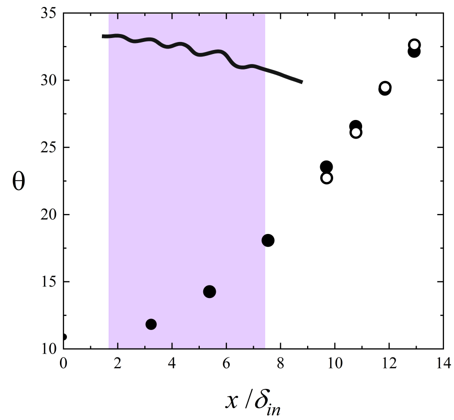


Figure 4. Comparison of momentum loss thickness distributions. The open symbol is marked as a wavy wall case, while dark symbols correspond to the unmodified wing surface.

Table 2. Integrated $C_f$ difference

| Integration [m] | $\Delta x_{t,s}$ [m] | $\Delta x_{t,s}\delta_{in}^{-1}$ [-] | $\Delta C_f$ [%] |
|---|---|---|---|
| 0.7 - 1.3 | 0.21 | 2.32 | 42.3 |

To assess the reduction in velocity deficit in the wake of the airfoil, it is instructive to examine the evolution of the momentum-loss thickness, $\theta$. An effective separation control strategy should not merely redistribute momentum toward the wall but rather preserve or enhance the total momentum within the boundary layer. In this context, $\theta$ serves as a robust integral measure for quantifying the net momentum retention downstream of the control intervention. In Figure 4, the distributions of $\theta$ for the wavy surface (open symbols) are compared with the distributions of $\theta$ as a function of $x\delta_{in}^{-1}$ on the unmodified wing surface (dark symbols). Symbols as in Figure 3.

The results shown in Figure 4 indicate a maintenance of overall momentum by the wavy wall. Other parameters indicating the effectiveness of the proposed flow control method are presented in Figure 5. The primary parameter most af-

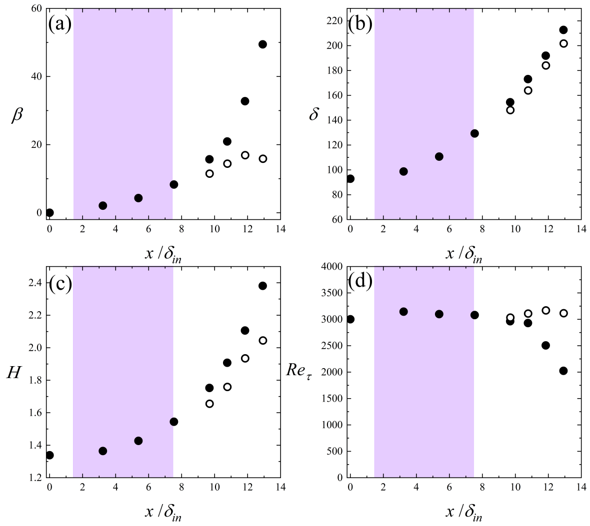


Figure 5. Comparison of $\beta$ a), $\delta$ b), $H$ c) and $Re_\tau$ d) downstream the flow.

fected is $\beta$ as it includes the wall shear stress that is strongly influenced (see Figure 5a). The distributions show a considerable decrease in the value of $\beta$ as a result of the impact of wavy wall. The increase in strain rate, which is proportional to the wall shear stress, is also reflected in the reduction in the thickness of the TBL (see Figure 5b) and in the shape factor $H$ (see Figure 5c). Interestingly, the Reynolds number $Re_\tau$ distributions observed above $\beta \approx 15$ (see Figure 5d) show that the wavy wall do not cause a visible decrease in $Re_\tau$ downstream of WW.

Since the thickness of the boundary layer for this location is approximately 5% lower (see Figure 5), the increase in the linear measure of momentum-loss thickness observed in the final profile (at $x = 1200$ mm) does not directly translate into an increase in the width of the wake as the wake behind the airfoil is defined in the plane perpendicular to the main flow direction. In addition, the wake velocity deficit is reduced as the boundary layer develops on both the suction and pressure sides of the airfoil. The wavy geometry promotes the reduction by enhancing momentum near the wall on the upper surface, thereby minimising the imbalance between the two boundary layers.

To confirm the above statement and to gain a more detailed insight into the flow field modified by the wavy wall, the profiles of mean velocity and streamwise Reynolds stress downstream the flow are shown in Figure 6. Note that the profiles are normalised by the edge velocity $U_e$. The streamwise evolution of these profiles is shown at the locations $x = 900$ mm, $x = 1000$ mm, $x = 1100$ mm, and $x = 1200$ mm on the surface. The black symbols correspond to the profiles measured on the unmodified wing surface, while the open symbols represent the profiles for the WW case.

All mean velocity profiles (obtained on the unmodified wing surface and the surface with the wall undulations) collapse in the outer region, which means that the wavy wall only affects the inner region of the boundary layer, where a marked increase in mean velocity is observed. It can be concluded that the characteristic behaviour of the mean profile when we deal with the effective flow control strategy is a decrease in the wake region. Figure 6a at $x = 900mm$ shows that the $\overline{uu}U_e^{-2}$ is leverage due to the wavy wall, and it decays downstream, which is visible for $x = 1000$ mm and 1100 mm profiles. For

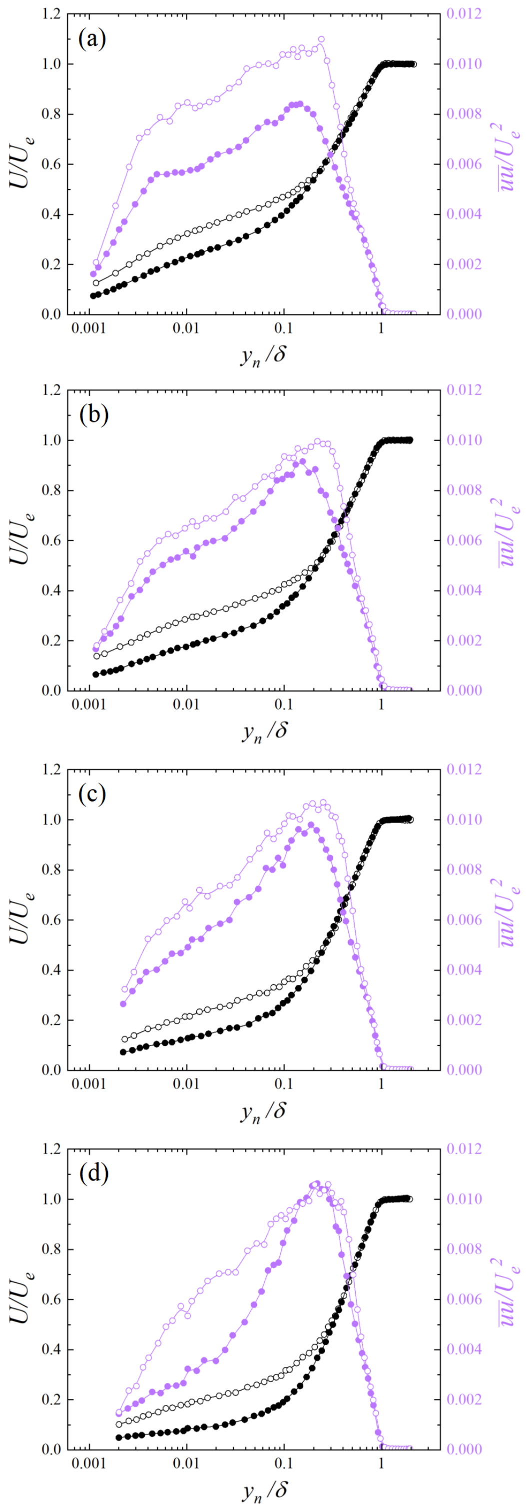


Figure 6. Comparison of the mean velocity and velocity variance components: $x = 900$ mm a), $x = 1000$ mm b), $x = 1100$ mm c) and $x = 1200$ mm d).

the last profile (Fig. 6d), the level of $\overline{uu}U_e^{-2}$ for the unmodified case drops significantly, which is caused by the fact that the flow is close to separation. A direct comparison between $\overline{uu}U_e^{-2}$ profiles indicates that the wavy surface is responsible for flattening the outer maximum. The flattening rate increases with increasing $x$. There is also a noticeable increase in $\overline{uu}U_e^{-2}$

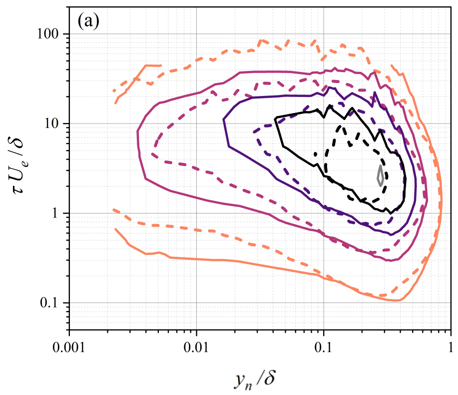


Figure 7. Premultiplied energy spectra comparison at location $x = 1100$ mm. Solid lines original WW and dashed contours wing profile surface. Increments marked by colours between iso-contour levels equal 0.0005.

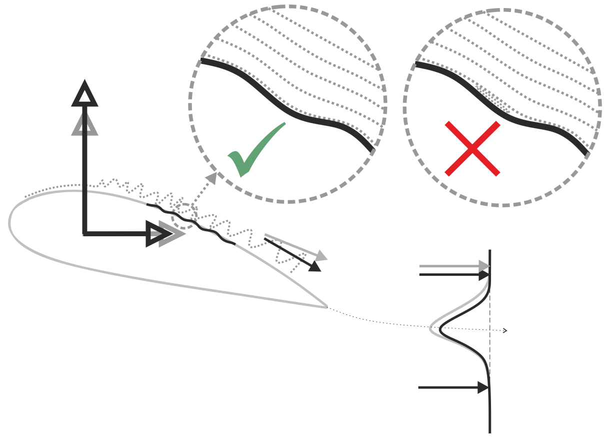

Figure 8. Schematic mechanism of the wavy wall at high Reynolds numbers. The dark colour corresponds to the characteristics (lift force, drag force, and wake) of a wavy wall with a flow at the verge of separation in troughs.

distributions in the near-wall region. This effect can be attributed to the change in the flow history of the pressure gradient, as the distribution $\beta$ (see Figure 5) is weaker for a wavy wall, causing the outer maximum to shift away from the wall (Bobke *et al.*, 2017).

According to Atzori *et al.* (2020), who studied suction and blowing applied on the suction side of the airfoil, an 11% increase in the lift-to-drag ratio can be achieved by reducing wall-normal convection on the suction side using suction. The reduction in $\delta$ in Fig 4b) indicates a decrease in wall-normal convection. This is consistent with the findings of Atzori *et al.* (2020), which show that it reduces total drag by substantially reducing pressure drag. This indicates that the baseline $C_d = 0.009$ of an airfoil at AoA of 5° for $Re_c = 10^7$ can be reduced by the wavy wall. Although, the exact increase in the lift coefficient $C_l$ remains undetermined, a tangential shift in the flow separation point quantified as $\Delta x_{t,s} c^{-1} = 8.3\%$, where $c$ is the chord of the applied wing section, can be associated with at least 5% increase in lift, which is considered a huge improvement in the aerodynamic performance of the airfoil at this Reynolds number.

The physical mechanism of an increase in momentum by a wavy wall was discussed in Dróżdż *et al.* (2025) in the aspect of small-scale activity. The key condition to promote momentum increasing wavy wall is high energy of small scales over the wavy surface flown without the separation in through. In particular, it was also concluded that the dominant influence of large-scale motions, manifested as an outer peak in the streamwise Reynolds stress that exceeds the energy of the inner peak, indicates a shift of energy across the turbulence scales. When small-scale activity remains elevated, it signifies enhanced momentum transport induced by the wavy wall.

To explain the role of small and large scales fractional energy contribution in the flow, the iso-contours of the wavelet energy spectra $E_{uu}$ (equivalent to the pre-multiplied energy spectra) are presented in Figure 7 for the same location for this cases. The reduced wavelet energy spectra $E_{uu}U_e^{-2}$ are presented as a function of the normalised time scale $\tau U_e \delta^{-1}$ and the normalised wall distance $y\delta^{-1}$. In Figure 7a), an increase in large-scale energy across the TBL thickness and a small-scale energy increase near the wall due to WW (solid line) is observed.

Summing up, the Figure 8 presents the momentum increase mechanism induced by the wavy-wall, provided that there is no flow separation in the trough at a high Reynolds number. This condition promotes the largest difference between the mean flow and the convection of small scales on the downhill sides of WW, increasing the sweeping motion, thus the increase in near-wall momentum downstream. This mechanism also reduces wall-normal convection, as indicated by a less deflected velocity vector from the airfoil surface, as evidenced by lower $\delta$. It was confirmed by Atzori *et al.* (2020), that the reduced wall-normal convection promotes a momentum redistribution to the near-wall region of the airfoil suction surface, directly decreasing the deficit in the wake of the airfoil.

## CONCLUSIONS

A detailed experimental study shows that the addition of a wavy wall to a convex surface, in the specified location, may constitute a previously unexamined passive method to alter aerodynamic behaviour. It provides a new approach to delay flow separation and improve airfoil performance at high Reynolds numbers.

The presence of the wavy surface leads to a substantial rise in the skin-friction coefficient. Comparative results show that the selected corrugation shape may produce even a 42.3% increase over the integration region extending from the end of the wavy wall to the location where separation would begin on a smooth, unmodified surface. A significant outcome is the tangential shift in the flow separation point by 8.3% of the chord, which is roughly associated with about a 5% increase in lift for an airfoil at the given Reynolds number. This represents a substantial improvement in aerodynamic performance, primarily due to sustained momentum loss thickness and a 5% reduction in turbulent boundary layer thickness, indicating that the wall-normal convection is decreased due to an increase of streamwise convection caused by the wavy wall. Mean velocity profiles show a notable increase in the inner part, along with a noticeable rise in Reynolds stress distributions and flattening of the outer maximum due to waviness occupying the near-wall region. Furthermore, an increase in strain rate also contributes to a reduction in the shape factor $H$. At the same time, the value of $Re_\tau$ remains at a constant level further downstream of the wavy wall, contrasting with observations on the unmodified section of the wing.

In essence, the wavy surface, when precisely tuned, acts as a sophisticated flow control mechanism, effectively increasing skin friction and postponing flow separation, thus enhancing lift without a detrimental impact on overall airfoil drag, through favourable modifications to the boundary layer structure and momentum management.

Future studies will investigate the enhanced performance achieved through the use of other wave geometries, including a non-harmonic wave type on a curved surface resembling a blade surface.

## ACKNOWLEDGMENTS

The investigation was supported by National Science Centre under Grant No. DEC-2020/39/B/ST8/01449 and Statutory Fund BS/PB-1-100-301/2026/P.

## REFERENCES

Aoki, K., Muto, K. & Okanaga, H. 2012 Mechanism of drag reduction by dimple structures on a sphere. *Journal of Fluid Science and Technology* **7** (1), 1–10.

Atzori, Marco, Vinuesa, Ricardo, Fahland, Georg, Stroh, Alexander, Gatti, Davide, Frohnapfel, Bettina & Schlatter, Philipp 2020 Aerodynamic Effects of Uniform Blowing and Suction on a NACA4412 Airfoil. *Flow, Turbulence and Combustion* **105**, 735–759.

Bearman, P. W & Harvey, J. K 1976 Golf ball aerodynamics. *Aeronautical Quarterly* **27** (2), 112–122.

Belamadi, R., Djemili, A.b, Ilinca, A. & Mdouki, R. 2016 Aerodynamic performance analysis of slotted airfoils for application to wind turbine blades. *Journal of wind engineering and industrial aerodynamics* **151**, 79–99.

Bobke, A., Vinuesa, R., Örlü, R. & Schlatter, P. 2017 History effects and near equilibrium in adverse-pressure-gradient turbulent boundary layers. *Journal of Fluid Mechanics* **820**, 667–692.

Bravo-Mosquera, P. D., Catalano, F. M. & Zingg, D. W. 2022 Unconventional aircraft for civil aviation: A review of concepts and design methodologies. *Progress in Aerospace Sciences* **131** (December 2021).

Coder, J. G & Somers, D. M 2020 Design of a slotted, natural-laminar-flow airfoil for commercial transport applications. *Aerospace Science and Technology* **106**, 106217.

Dróżdż, A., Niegodajew, P., Romańczyk, M. & Elsner, W. 2023 Convection velocity in turbulent boundary layers under adverse pressure gradient. *Experimental Thermal and Fluid Science* p. 110900.

Dróżdż, A., Niegodajew, P., Romańczyk, M., Sokolenko, V. & Elsner, W. 2021 Effective use of the streamwise waviness in the control of turbulent separation. *Experimental Thermal and Fluid Science* **121**, 110291.

Dróżdż, A., Sokolenko, V. & Elsner, W. 2025 Performance analysis of novel wavy-wall-based flow control method for wind turbine blade. *Experimental Thermal and Fluid Science* **169** (March), 111527.

Elsner, W., Dróżdż, A., Szymanek, E., Tyliszczak, A. & Niegodajew, P. 2022 Experimental and numerical studies of turbulent flows over two-dimensional and three-dimensional rough surfaces under an adverse pressure gradient. *Applied Mathematical Modelling* **106**, 549–566.

Gattere, F., Chiarini, A.o & Quadrio, M. 2022 Dimples for skin-friction drag reduction: status and perspectives. *Fluids* **7** (7), 240.

Kamiński, P., Niegodajew, P., Dróżdż, A., Sokolenko, V., Tyliszczak, A. & Elsner, W. 2024 Numerical analysis of novel wavy wall based control of turbulent boundary layer separation. *Aerospace Science and Technology* **149**, 109167.

Kamiński, P., Tyliszczak, A., Elsner, W. & Niegodajew, P. 2025 Turbulent separation control with a tilted wavy wall: A promising approach for energy savings in aerodynamic systems. *Energy* **324**, 135758.

Mathis, R., Monty, J. P, Hutchins, N. & Marusic, I. 2009 Comparison of large-scale amplitude modulation in turbulent boundary layers, pipes, and channel flows. *Physics of Fluids* **21** (11), 111703.

McMasters, J. H & Henderson, M. L 1979 Low-speed single-element airfoil synthesis. *NASA. Langley Res. Center The Sci. and Technol. of Low Speed and Motorless Flight, Pt. 1* .

Monkewitz, P. A., Chauhan, Kapil A. & Nagib, Hassan M. 2007 Self-consistent high-reynolds-number asymptotics for zero-pressure-gradient turbulent boundary layers. *Physics of Fluids* **19** (11), 115101.

Mostafa, W., Abdelsamie, A., Sedrak, M., Thévenin, D. & M., M. H 2022 Quantitative impact of a micro-cylinder as a passive flow control on a horizontal axis wind turbine performance. *Energy* **244**, 122654.

Ricco, P., Skote, M. & Leschziner, M. A. 2021 A review of turbulent skin-friction drag reduction by near-wall transverse forcing. *Progress in Aerospace Sciences* **123**, 100713.

S., Seong-Ho & H., Cheol-Hyun 2016 Performance improvement of airfoils for wind blade with the groove. *International Journal of Green Energy* **13** (1), 34–39.

Sanmiguel Vila, C., Vinuesa, Ricardo, Discetti, S., Ianiro, A., Schlatter, P. & Örlü, Ramis 2017 On the identification of well-behaved turbulent boundary layers. *J. of Fluid Mech.* **822** (May), 109–138.

Sayed, M. A., Kandil, Hamdy A. & Morgan, El-Sayed I. 2012 Computational fluid dynamics study of wind turbine blade profiles at low reynolds numbers for various angles of attack. *AIP Conference Proceedings* **1440**, 467 – 479, cited by: 3.

Tanürün, H. E., Yıldız, A. & Seyhan, M. 2026 Aerodynamic performance analysis of a naca 63(4)-421 airfoil equipped with a trailing edge slot at suction side. *Experimental Thermal and Fluid Science* **171**, 111604.

Tay, C 2011 Determining the effect of dimples on drag in a turbulent channel flow. In *49th AIAA Aerospace Sciences Meeting Including the New Horizons Forum and Aerospace Exposition*, p. 682.

Tay, CMJ, Khoo, BC & Chew, YT 2015 Mechanics of drag reduction by shallow dimples in channel flow. *Physics of Fluids* **27** (3).

Wang, J.-S., Wu, J. & Wang, [redacted].-J. 2023 Wake-triggered secondary vortices over a cylinder/airfoil configuration. *Experiments in Fluids* **64** (1), 6.

Wang, Y., Li, G., S.Shen, Huang, D. & Zheng, Z. 2018 Influence of an off-surface small structure on the flow control effect on horizontal axis wind turbine at different relative inflow angles. *Energy* **160**, 101–121.